Interfacial instability in non-Newtonian fluid layers

N. J. Balmforth
Department of Applied Mathematics and Statistics, University of California at Santa Cruz, California 95064

R. V. Craster
Department of Mathematics, Imperial College, London SW7 2BZ, United Kingdom

C. Toniolo
Dipartimento di Ingegneria Ambientale, Università di Genova, Via Montallegro 1, 16145 Genova, Italy

(Received 15 April 2003; accepted 29 July 2003; published 22 September 2003)

Superposed layers of fluid flowing down an inclined plane are prone to interfacial instability even in the limit of zero Reynolds number. This situation can be explored by making use of a lubrication-style approximation of the governing fluid equations. Two versions of the lubrication theory are presented for superposed layers of non-Newtonian fluid with power-law rheology. First, the fluids are assumed to have comparable effective viscosities. The approximation then furnishes a simplified model for which the linear stability problem can be solved analytically and concisely. Weakly nonlinear analysis and numerical computations indicate that instabilities saturate at low amplitude beyond onset and form steady wavetrains. Further from onset, secondary instabilities arise that destroy trains of widely spaced wave trains. Patterns of closely spaced waves, on the other hand, coarsen due to wave merger events. The two mechanisms select steady wavetrains with a characteristic spatial scale. The second lubrication theory assumes that the upper layer is far more viscous than the lower layer. As a result, the upper fluid flows almost rigidly, and extensional stresses can become promoted into the leading-order balance of forces. Interfacial instability still arises in Newtonian fluid layers, and the nonlinear dynamics is qualitatively unchanged. Significant complications arise when the upper fluid is non-Newtonian due to the behavior of the viscosity at zero strain rate. © *2003 American Institute of Physics.* [DOI: 10.1063/1.1611179]

I. INTRODUCTION

As vividly illustrated by windows and gutters on rainy days and by many water sculptures, thin films of fluid flowing down inclined planes are unstable to the formation of wave patterns. In this phenomenon, sometimes referred to as the Kapitza problem, the instability operates by draining fluid into locally thicker features that move relative to the film and sweep up further fluid from the surrounding film as they propagate. The instability appears at much lower Reynolds numbers than those typically required for a transition to turbulence. Nevertheless, the wave patterns can show a rich variety of behavior both in space and time, and have provided fluid mechanicians and nonlinear dynamicists much food for thought over the last fifty or so years.

The critical Reynolds number for the onset of instability can be determined by linear stability theory. In falling fluid films, the analysis is performed analytically using long-wave expansions because the most unstable waves typically have the largest spatial scales in the plane of the film.[1,2] The theory was further generalized to finite-amplitude long waves by Benney,[3] and his nonlinear equation (together with variants derived later by a host of other authors), has provided the basis of many studies of spatio-temporal complexity in the wave patterns of falling liquid films.[4]

In this article, we consider instability in multiple, superposed fluid layers. Such situations were previously considered by Chen,[5] Weinstein,[6] and others. Because each individual layer is not so different to a single layer, one expects instabilities in such films when the Reynolds number is sufficiently high. However, superposed layers also have the additional degree of freedom associated with motions of the interfaces inside the fluid composite. Such interfacial motions have been shown to be a source of instability,[5,7] with discontinuities in shear stress being held responsible.[8] However, inertia is essential to the mechanism proposed and does not operate in the zero Reynolds number limit. Yet, multiple films can be unstable even in the inertia-less regime, as pointed out by Loewenherz and Lawrence.[9] We explore exclusively the zero-Reynolds number limit in the present paper, which allows us to take advantage of a lubrication-style approximation of the governing fluid equations. We present a coherent picture of the linear stability and extend the theory into the nonlinear regime to explore the nonlinear saturation and dynamics of unstable waves. A related model was derived previously by Kliakhandler and Sivashinsky.[10]

A further direction that we take in this study is to consider non-Newtonian fluid layers. Specifically, we study interfacial instability in two superposed layers of power-law fluid. Weinstein[6] has previously presented a few results on this stability using long-wave expansions; we offer a more complete discussion of how shear thinning or thickening affects stability in the inertia-less limit. The non-Newtonian problem has applications in chemical engineering, where layered flows arise in many coating processes, such as the manufacturing of plates of photographic emulsions and in

 © 2003 American Institute of Physics

Downloaded 15 Feb 2006 to 137.82.49.199. Redistribution subject to AIP license or copyright, see http://pof.aip.org/pof/copyright.jsp

various extrusion and transport processes. Interfacial instability in two-layer flows of power-law fluid in channels has been considered earlier.[11,12]

The non-Newtonian problem is also relevant to glaciology, where ice is thought to act like a power-law fluid (the rheology is more commonly referred to as Glen's law in the glaciological literature), and, in some situations, slides over a much less viscous mud layer. This scenario is particularly relevant to ice streams, where localized, relatively fast-moving flows develop within more extensive, slowly moving ice sheets, and various observations indicate that the ice streams slide over an unconsolidated sediment.[13] Previously, Loewenherz and Lawrence[9,14] suggested that interfacial instabilities may play a role in glacier variability, although their main focus was upon rock glaciers. Our original motivation for the current work was to continue in this vein and explore whether ice stream formation and variability could be connected to interfacial waves. However, we deal with a highly idealized fluid model here, which misses much of the essential physics that plays a role in ice-stream dynamics (for example, glaciers and ice sheets have a complicated basal structure involving channels of draining meltwater, embedded rock and sediment eroded from the ground underneath, which is for responsible for allowing the ice mass to slide at its base[15]). In our conclusions we remark further on the relevance of our results to ice streams.

A key detail of the glacier problem that requires an interesting extension of the theory, is that the upper layer may have a much larger effective viscosity than the lower layer. The physical ramification of this disparity is that the upper layer slides almost rigidly over the much more fluid layer beneath; the shear is almost entirely taken up in the lower layer. However, besides suppressing the shear in the upper layer, the enhancement in viscosity can further promote extensional stresses which resist divergence or convergence of flow. Such stresses are missing in the usual lubrication analysis of flow over a plane because they normally lie at higher order than the vertical viscous stress. In the current situation, when the extensional stresses are of the same order as the vertical viscous stress, we must revise the original asymptotic scheme. The modified lubrication theory is somewhat analogous to that used to describe free films,[16] viscous threads,[17] and ice shelves and streams.[18] Using this second model, we explore the effect of the extensional stresses on interfacial instability.

II. FORMULATION OF THE MODEL

A. The equations

We consider two superposed layers of incompressible and immiscible materials flowing down an inclined plane, as shown in Fig. 1. A Cartesian coordinate system aligned with the plane describes the fluid; x points down the slope, and z is perpendicular to it. The material properties of the two layers are different; we use subscripts to distinguish them. For example, ρ_1 and ρ_2 denote the densities in the upper and lower fluids, respectively. In z, the lower layer has thickness, $\zeta(x,t)$, and the upper layer has depth, $\theta(x,t)$; the composite has thickness, $h(x,t)=\zeta(x,t)+\theta(x,t)$. The flow is described

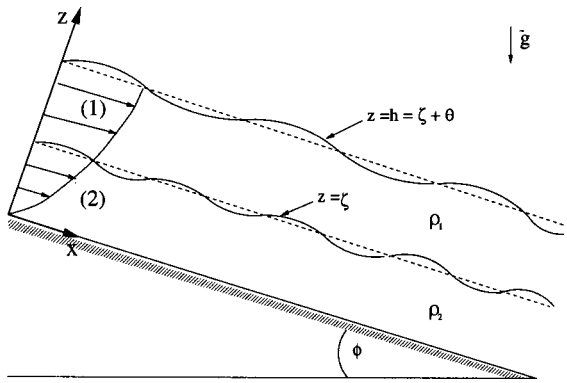

FIG. 1. The two layer model. The upper and lower fluids are incompressible, with constant densities ρ_1 and ρ_2. The angle ϕ fixes the slope of the plane. ζ is the thickness of the lower layer, θ that of the upper layer, and $h=\theta+\zeta$ is total thickness.

by the velocity field $(u(x,z,t),w(x,z,t))$, and pressure $p(x,z,t)$. Surface tension (though easily incorporated) is neglected both on the free surface and the dividing interface.

The governing equations are given by conservation of momentum,

$$\rho_j(u_t+uu_x+wu_z)=-p_x+(\partial_x\tau_{xx}+\partial_z\tau_{xz})+\rho_j g\sin\phi, \tag{1}$$

$$\rho_j(w_t+uw_x+ww_z)=-p_z+(\partial_x\tau_{xz}+\partial_z\tau_{zz})-\rho_j g\cos\phi \tag{2}$$

for $j=1$ and 2, and continuity,

$$u_x+w_z=0, \tag{3}$$

where partial derivatives have been written as (x,z) subscripts, $\mathbf{g}=(g\sin\phi,-g\cos\phi)$ is the gravitational acceleration, and τ_{lm} are the components of the deviatoric stress tensor, the total tensor being $\mathbb{T}=\tau-p\mathbb{I}$.

We impose a no-slip boundary condition on the inclined plane:

$$u=w=0 \quad \text{on} \quad z=0. \tag{4}$$

At the fluid interface, $z=\zeta$, we require continuity of velocities, the kinematic condition of the material surface, and the balance of the normal and tangential stresses:

$$u(x,\zeta^-,t)=u(x,\zeta^+,t)=u_I(x,t), \tag{5}$$

$$w(x,\zeta^-,t)=w(x,\zeta^+,t)=w_I(x,t)=\zeta_t+u_I\zeta_x, \tag{6}$$

$$\mathbb{T}(x,\zeta^-,t)\cdot\begin{pmatrix}-\zeta_x\\1\end{pmatrix}=\mathbb{T}(x,\zeta^+,t)\cdot\begin{pmatrix}-\zeta_x\\1\end{pmatrix}, \tag{7}$$

where subscript I refers to interfacial speeds. At the upper surface, $z=h$, we again apply the kinematic condition and continuity of stress:

$$h_t+u(x,h,t)h_x=w(x,h,t), \tag{8}$$

$$\mathbb{T}(x,h,t)\cdot\begin{pmatrix}-h_x\\1\end{pmatrix}=\mathbf{0}, \tag{9}$$

which ignores any interaction with the overlying air.

For the constitutive relation, we adopt a power-law rheology,

Downloaded 15 Feb 2006 to 137.82.49.199. Redistribution subject to AIP license or copyright, see http://pof.aip.org/pof/copyright.jsp

$$\tau_{kl}=K_j\dot{\gamma}^{n_j-1}\dot{\gamma}_{kl}\equiv\mu_j(\dot{\gamma})\dot{\gamma}_{kl}, \tag{10}$$

where

$$\dot{\gamma}_{kl}\equiv\begin{pmatrix} 2u_x & u_z+w_x \\ u_x+w_z & 2w_z \end{pmatrix}, \quad \dot{\gamma}=\sqrt{\tfrac{1}{2}\dot{\gamma}_{kl}\dot{\gamma}_{lk}}, \tag{11}$$

and the rheology is each layer is given by the consistency, K_j, and a power-law index, n_j [$\mu_j(\dot{\gamma})$ is an effective viscosity]. If $n_j=1$ for $j=1$ or 2, then that fluid is Newtonian.

B. Nondimensionalization

We remove dimensions from the governing equations as follows: We define H as a characteristic thickness of the composite fluid layer and measure downslope lengths with the unit, L. We scale velocities (u,w) with the characteristic speeds, U and UH/L, and time t with L/U:

$$x=L\tilde{x}, \quad z=H\tilde{z}, \quad u=U\tilde{u}, \quad w=UH\tilde{w}/L, \quad t=L\tilde{t}/U, \tag{12}$$

where the tilde indicates dimensionless variables. For pressure, we take $p=\rho_1 gH\tilde{p}\cos\phi$, and we scale the strain rates with the unit, U/H. The leading-order balance between downslope pressure gradients and the shear stress selects the velocity scale, $U=(\rho_1 gH^{2+n_2}\cos\phi/K_2L)^{1/n_2}$.

The lubrication theory proceeds by defining $\epsilon=H/L$ as the characteristic aspect ratio of the layers, and requiring this ratio to be small: $\epsilon\ll 1$. We further assume that the principal force balance arises between pressure gradients and viscous stresses in the downslope direction, and inertial effects are weaker. Thus we insist that $\mathrm{Re}=\rho_1 UL/K_2$, the Reynolds number of the flow based on the downslope lengthscale, be of order unity or smaller. The dimensionless form of the momentum equations, dropping the tilde superscript, is then

$$\epsilon^2 D_j\,\mathrm{Re}(u_t+uu_x+wu_z)=-p_x+\epsilon\partial_x\tau_{xx}+\partial_z\tau_{xz}+SD_j, \tag{13}$$

$$\epsilon^4 D_j\,\mathrm{Re}(w_t+uw_x+ww_z)=-p_z+\epsilon^2\partial_x\tau_{xz}+\epsilon\partial_z\tau_{zz}-D_j. \tag{14}$$

In the equations above $D_j=\rho_j/\rho_1$ is the density ratio, and $S=(L/H)\tan\phi$ is a slope parameter, assumed order one (so the plane has a gentle inclination). The continuity equation remains unchanged.

The dimensionless strain rates are given by

$$\dot{\gamma}_{kl}\equiv\begin{pmatrix} 2\epsilon u_x & u_z+\epsilon^2 w_x \\ u_z+\epsilon^2 w_x & 2\epsilon w_z \end{pmatrix},$$

$$\dot{\gamma}=[(u_z+\epsilon^2 w_x)^2+4\epsilon^2 u_x]^{1/2}. \tag{15}$$

The deviatoric stress components can then be written in the form,

$$\tau_{kl}=\begin{cases} R^{-1}\dot{\gamma}^{(n_1-1)}\dot{\gamma}_{kl}, & \zeta\leqslant z\leqslant h, \\ \dot{\gamma}^{(n_2-1)}\dot{\gamma}_{kl}, & 0\leqslant z\leqslant\zeta, \end{cases} \tag{16}$$

where $R=(K_2/K_1)(U/H)^{n_2-n_1}$ is a ratio of dimensional, effective viscosities.

It is straightforward to re-express the boundary conditions in dimensionless form. Only the stress relations differ from their dimensional counterparts:

$$[\tau_{xz}-\epsilon(\tau_{xx}-p)\zeta_x]_{z=\zeta^-}^{z=\zeta^+}=[\tau_{zz}-p-\epsilon\tau_{xz}\zeta_x]_{z=\zeta^-}^{z=\zeta^+}=0,$$
$$[\tau_{xz}-\epsilon(\tau_{xx}-p)h_x]_{z=h}=[\tau_{zz}-p-\epsilon\tau_{xz}h_x]_{z=h}=0. \tag{17}$$

C. The lubrication model

We now retain only the leading-order terms of the dimensionless equations. The momentum equations become

$$0=-p_x+\partial_z\tau_{xz}+SD_j \quad \text{and} \quad 0=-p_z-D_j, \tag{18}$$

which integrate to

$$p=\begin{cases} h-z, & \zeta<z<h, \\ h-\zeta+D(\zeta-z), & 0<z<\zeta, \end{cases}$$

and

$$\tau_{xz}=\begin{cases} (S-h_x)(h-z), & \zeta<z<h, \\ \Delta_x(\zeta-z)+\tau_I, & 0<z<\zeta, \end{cases} \tag{19}$$

where $D=D_2=\rho_2/\rho_1$ and

$$\tau_I=(S-h_x)\theta, \quad \Delta_x=SD-\theta_x-D\zeta_x. \tag{20}$$

Given the stresses, the constitutive relation (16) now yields

$$u_z=\begin{cases} R^{1/n_1}(S-h_x)^{1/n_1}(h-z)^{1/n_1}, & \zeta<z<h, \\ [\Delta_x(\zeta-z)+\tau_I]^{1/n_2}, & 0<z<\zeta. \end{cases} \tag{21}$$

A further integral provides the relation,

$$u_I=\frac{n_2}{n_2+1}\frac{1}{\Delta_x}[\tau_B^{1+1/n_2}-\tau_I^{1+1/n_2}], \quad \tau_B=\tau_I+\Delta_x\zeta. \tag{22}$$

Finally, we combine integrals of the continuity equation with the kinematic conditions of the surfaces $z=\zeta$ and $z=h$

$$\theta_t+\partial_x\left[\int_\zeta^h u_z(h-z)dz+u_I\theta\right]=\zeta_t+\partial_x\left[\int_0^\zeta u_z(\zeta-z)dz\right]=0. \tag{23}$$

On substituting the form of the velocity field, we find

$$\theta_t+R^{1/n_1}\partial_x\left[\frac{n_1\tau_I^{1/n_1}\theta^2}{2n_1+1}\right]+\frac{n_2}{n_2+1}\partial_x\left[\frac{\theta}{\Delta_x}(\tau_B^{1+1/n_2}-\tau_I^{1+1/n_2})\right]=0, \tag{24}$$

$$\zeta_t+\frac{n_2}{n_2+1}\partial_x\left[\frac{\zeta\tau_B^{1+1/n_2}}{\Delta_x}+\frac{n_2}{2n_2+1}\times\frac{1}{\Delta_x^2}(\tau_I^{2+1/n_2}-\tau_B^{2+1/n_2})\right]=0. \tag{25}$$

III. LINEAR STABILITY

The system admits a steady flow solution with a flat interface and free surface: $\zeta=Z$, $\theta=\Theta$ and $h=1=\Theta+Z$. We explore the linear stability of this solution by introducing the normal-mode form,

$$(\zeta,\theta)=(Z,\Theta)+[(\hat{\zeta},\hat{\theta})e^{ikx+\lambda t}+\text{c.c.}], \tag{26}$$

Downloaded 15 Feb 2006 to 137.82.49.199. Redistribution subject to AIP license or copyright, see http://pof.aip.org/pof/copyright.jsp

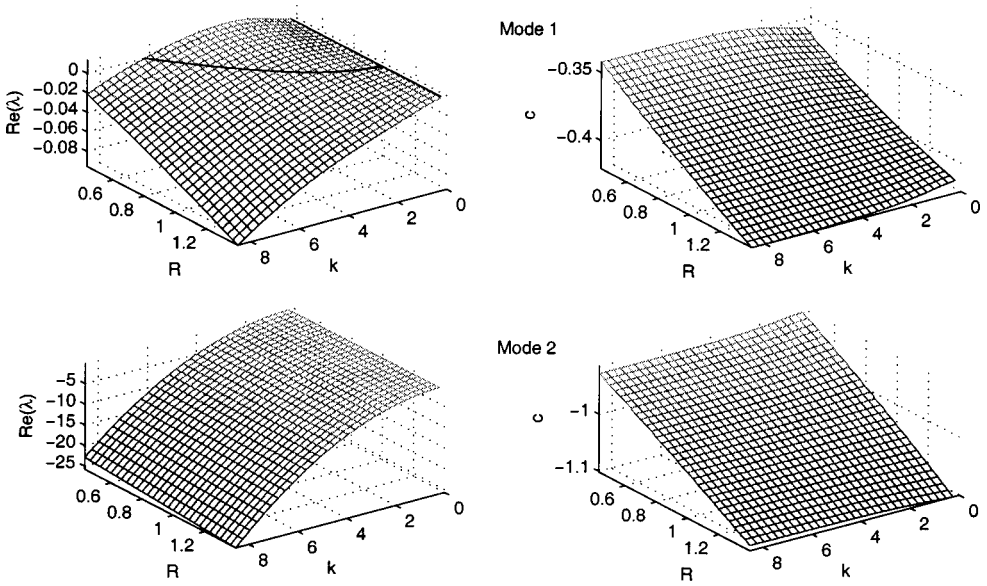

FIG. 2. Shown are growth rates, $\mathrm{Re}(\lambda_l)$, and wavespeeds, $c=-\mathrm{Im}(\lambda_l)/k$, of the two eigenmodes, $l=1$ and 2, as functions of wavenumber, k, and viscosity ratio, R, for $D=1.1$ and $\Theta=0.5$. The darker line in the first surface shows the curve of neutral stability.

into the model equations (24) and (25), and then linearizing in the perturbation amplitudes, $(\hat{\zeta},\hat{\theta})$. The result is an algebraic eigenvalue problem for the (complex) growth rate λ, solved as a function of the wavenumber k. If $\mathrm{Re}(\lambda)>0$ the equilibrium flow is unstable.

To minimize the number of free parameters in the stability problem, we fix $S=1$ by suitably selecting the downslope lengthscale: $L=H/\tan\phi$. In addition to the wavenumber k, this leaves five dimensionless parameters determining the stability properties: The effective viscosity ratio, R, the relative thickness of the upper layer, Θ, the density ratio, $D=\rho_2/\rho_1$, and the two "power-law" exponents, n_1 and n_2. We restrict attention to cases of stable density stratification, $D>1$, filtering out Rayleigh–Taylor instabilities.

A. The Newtonian case

A useful first step in exploring the linear stability is to consider the case of two viscous fluids ($n_1=n_2=1$); we fix $D=1.1$ and vary the other parameters. Figure 2 shows growth rates, $\mathrm{Re}(\lambda_i)$, and wavespeeds, $-\mathrm{Im}(\lambda_i)/k$, against wavenumber and R for $\Theta=0.5$. The flows with lower viscosity ratios are unstable over certain ranges of wavenumber, as found by Yih;[1] that is, when the bottom fluid is the less viscous. Of the two eigenvalues, only one becomes unstable, and the instability takes the form of long waves. Kao[19–21] presented similar results to those shown in Fig. 2, and also investigated the role of the density stratification, which we largely ignore here. In Fig. 3 we plot curves of neutral stability on the (k,R)—plane for several values of the upper layer thickness Θ. Below these curves, the equilibrium flow is unstable. The unstable region is largely contained in $R<1$. Surprisingly, an instability region also appears above the line of equal viscosities $R=1$ (a feature also noted by Kao). In the limiting cases, $\Theta=0$ and $\Theta=1$, representing the absence of one of the layers, one of the eigenvalues disappears and we are left with a single stable Newtonian layer.

Figure 4 displays the maximal growth rate over all k on the (R,Θ)-plane. Also shown is the wavenumber that maximizes the growth rate. Instability appears for all $0<\Theta<1$ and $R<1$, as well as inside the narrow window with R just greater than unity and small Θ. We conclude that the slightest viscosity contrast between the layers (in the sense that the upper layer is more viscous) can be destabilizing; the various parameters of the problem change the detailed linear instability, but not this qualitative conclusion.

B. Effects of a power law rheology

With power-law rheology, the effective viscosity can vary substantially across each of the superposed layers, making ambiguous the definition of the viscosity contrast between the two fluids (which controls the instability for Newtonian layers). We offer a rough guide to the effect of the rheology as follows. First consider a non-Newtonian layer

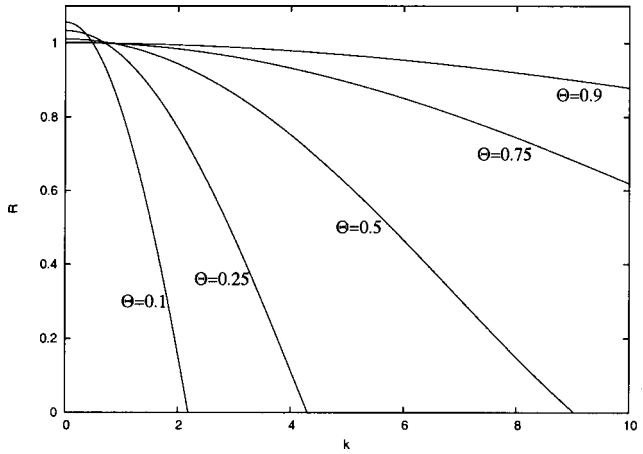

FIG. 3. Curves of neutral stability on the (k,R)—plane for $D=1.1$ and $\Theta=0.1$, 0.25, 0.5, 0.75, and 0.9. The equilibrium flow is unstable below these curves.

Downloaded 15 Feb 2006 to 137.82.49.199. Redistribution subject to AIP license or copyright, see http://pof.aip.org/pof/copyright.jsp

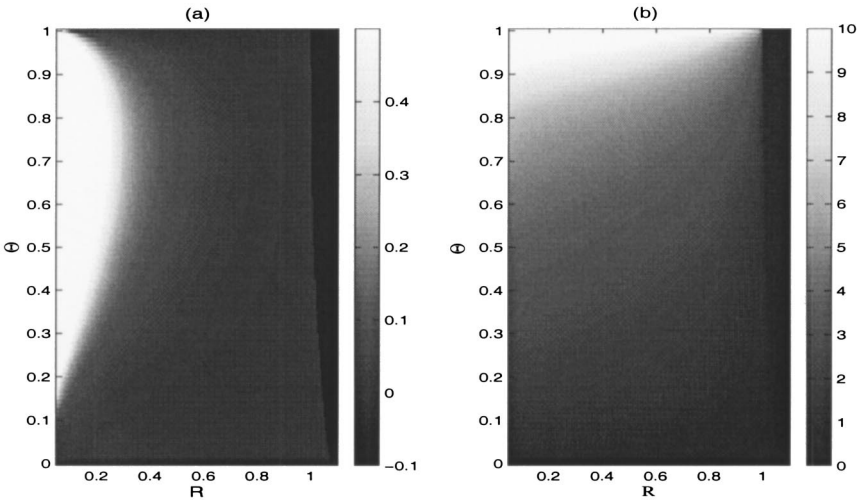

FIG. 4. (a) Maximum growth rate over all k and (b) the associated wavenumber on the (R,Θ)-parameter plane, for $D=1.1$, $n_1=1$, $n_2=1$. The dark area to the right locates the stable region, where the growth rate is negative for all k.

atop a Newtonian fluid. The dimensionless effective viscosity of the equilibrium flow follows from (21):

$$\nu_1(z)=R^{-1/n_1}(h-z)^{1-1/n_1}. \tag{27}$$

Given that the instability is an interfacial one, we assume that the important value of this viscosity is that at the interface. Thus we compare $\nu_1(Z)=R^{-1/n_1}\Theta^{1-1/n_1}$ with the viscosity of the lower layer (unity). Based on the results for Newtonian fluids, we then predict instability if the ratio of these two values exceeds unity:

$$\frac{\Theta^{1-1/n_1}}{R^{1/n_1}}>1 \quad \text{or} \quad R<\Theta^{n_1-1}. \tag{28}$$

In Fig. 5 we compare this simple prediction with numerical computation of the stability boundary (over all k) on the (R,Θ)-plane, and find qualitative agreement.[27] Since $\Theta<1$, when the upper fluid is shear-thinning ($n_1<1$), the viscosity is raised at the interface, promoting instability. Conversely, the interfacial viscosity is lowered for a shear-thickening upper layer, and the interface is more stable.

Similar considerations lead to an analogous prediction for a flow with a Newtonian layer above a non-Newtonian fluid. In this case, the mean effective viscosity in the lower layer is

$$\nu_2(z)=[\Theta+D(Z-z)]^{1-1/n_2}. \tag{29}$$

At the interface, $\nu_2(Z)=\Theta^{1-1/n_2}$, whereas the upper layer now has a viscosity of R^{-1}. Thus we anticipate instability when

$$R<\Theta^{1/n_2-1}. \tag{30}$$

Figure 6 compares this prediction with more numerical results; again there is qualitative agreement. Some more refined analytical predictions will be given momentarily.

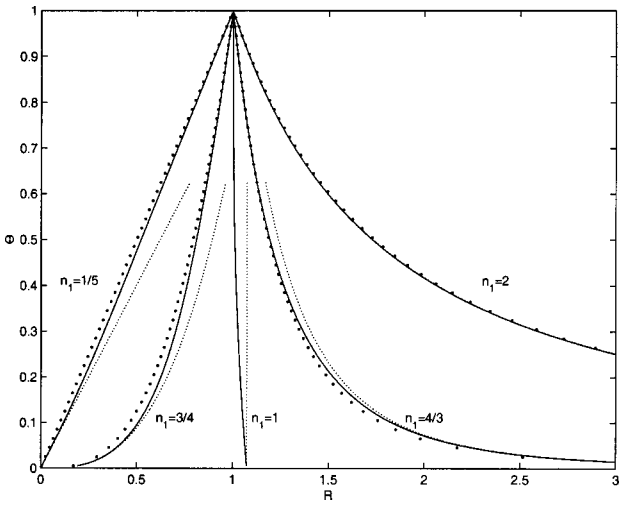

FIG. 5. Marginal stability curves for $D=1.1$, a lower Newtonian layer ($n_2=1$) and an upper non-Newtonian layer. Five cases are shown corresponding to upper layers that are shear-thickening ($n_1=4/3$ and 2), Newtonian ($n_1=1$), or shear-thinning ($n_1=1/5$ and 3/4). The dots show the prediction (28), and the dotted line is the prediction of the small Θ-expansion. For $n_1=2$ the three curves are hard to distinguish.

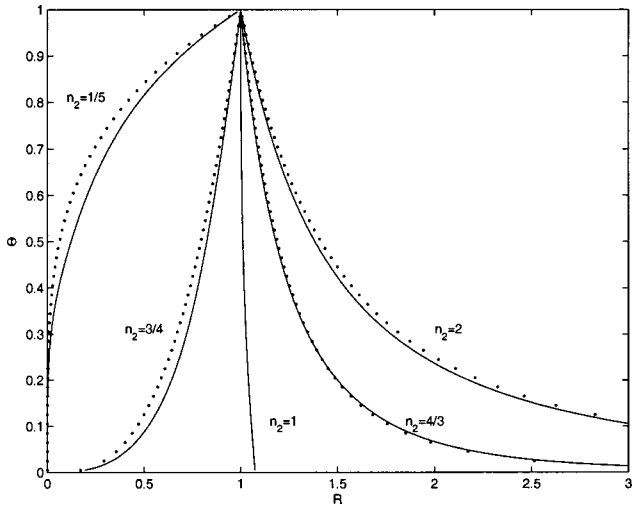

FIG. 6. Marginal stability curves for $D=1.1$, an upper Newtonian layer ($n_1=1$) and a lower non-Newtonian layer. The five curves show results for a lower layer that is shear-thickening ($n_2=4/3$ and 2), Newtonian ($n_2=1$) or shear-thinning ($n_2=1/5$ and 3/4). The dots show the prediction (30).

Downloaded 15 Feb 2006 to 137.82.49.199. Redistribution subject to AIP license or copyright, see http://pof.aip.org/pof/copyright.jsp

C. Thin basal fluid layer: Small Z

When $Z \ll 1$, we may reduce the lubrication model further and extract a simple stability criterion. In this limit, interfacial perturbations have amplitude of the order of the lower-layer thickness and develop slowly: $(\theta-\Theta,\zeta) \rightarrow O(Z)$ and $(\theta_t,\zeta_t)\rightarrow O(Z^2)$. The slow evolution demands that, to order Z in the θ-equation (24),

$$0 \sim \partial_x\left[\frac{n_1(R\tau_I)^{1/n_1}\theta}{2n_1+1}+u_I\theta\right]\sim\partial_x\left[R^{1/n_1}\theta+\zeta-\frac{R^{1/n_1}h_x}{1+2n_1}\right]. \tag{31}$$

That is, the flux of fluid through the upper layer remains constant in each vertical section to leading order; the upper flow adjusts instantaneously to deformations in the interface. Any disturbance in the interfacial speed must, therefore, be accompanied by changes in the thickness of the upper layer to maintain constant upper-layer flux. We now use the integral of (31)

$$\theta \sim \Theta + \frac{h_x}{1+2n_1}-\frac{\zeta-Z}{R^{1/n_1}}, \tag{32}$$

to write the ζ-equation (25) as

$$\zeta_t \sim \frac{1}{2}\partial_x\left[-\zeta^2-\frac{(1-R^{1/n_1})}{n_2R^{1/n_1}}Z\zeta^2+\frac{3-2DR^{1/n_1}}{3n_2R^{1/n_1}}\zeta^3 + \frac{2n_1\zeta^2h_x}{n_2(1+2n_1)}\right]+O(Z^4), \tag{33}$$

which constitutes the reduced system.

On linearizing, we read off the amplitude relation,

$$\hat{\theta}\sim\frac{ikR^{1/n_1}-(1+2n_1)}{R^{1/n_1}(1+2n_1-ik)}\hat{\zeta}, \tag{34}$$

and eigenvalue,

$$\lambda \sim -ikZ+\frac{ikZ^2[1-2R^{1/n_1}(D-1)]}{2n_2R^{1/n_1}} + \frac{n_1k^2Z^2(1-R^{1/n_1})(1+2n_1+ik)}{n_2R^{1/n_1}[(1+2n_1)^2+k^2]}. \tag{35}$$

Thus the system is unstable if $R<1$, independently of the values of n_1 and n_2, as seen in Figs. 5 and 6. From (33), we identify the term involving slope of the free surface, h_x, as that responsible for instability at $O(Z^2)$. Because $\hat{h}=\hat{\theta}+\hat{\zeta} \sim (1-R^{-1/n_1})\hat{\zeta}$ for small Z and long waves (the most dangerous disturbances to stability), the free surface moves out of phase with an interface perturbation if $R<1$. Physically, wherever an initial perturbation raises (depresses) the interface, the constancy of the upper-layer flux forces the free surface to become lowered (elevated). The resulting inclination of the free surface then changes the interfacial shear stress, which forces a flux in the lower layer that removes fluid from below the depressions of the interface, and adds fluid below interfacial elevations, thus strengthening the initial perturbation, and leading to instability.

From the nonlinear perspective, the leading-order term in (33) is the nonlinear wave-steepening term $\zeta\zeta_x$, whereas the linear instability appears at higher order. Thus, we anticipate that weak instability nucleates waves that steepen rapidly into shock-like structures. Indeed, in the numerical computations reported later, we observe this kind of dynamics at small Z.

D. Thin upper surface layer: Small Θ

The behavior of the system when $\Theta \ll 1$ depends sharply on the exponents n_1 or n_2; we explore the configuration with a Newtonian lower layer: When $n_2=1$, the key non-Newtonian term in the equations is

$$\frac{n_1R^{1/n_1}}{2n_1+1}\tau_I^{1/n_1}\theta^2=\frac{n_1R^{1/n_1}}{2n_1+1}(1-\theta_x-\zeta_x)^{1/n_1}\theta^{2+1/n_1}. \tag{36}$$

This term introduces nonintegral powers of Θ in a power series solution for small Θ. To avoid this complication, it is convenient to rescale the linearized system by defining a modified viscosity parameter $\tilde{R}$: $R=\tilde{R}^{n_1}\Theta^{n_1-1}$. This procedure eliminates nonintegral powers of Θ, and the solution then takes the form of a regular power series: $\lambda=\lambda_0+\lambda_1\Theta+\lambda_2\Theta^2+\lambda_3\Theta^3+\cdots$. We find

$$\mathrm{Re}(\lambda)\sim-\frac{k^4\Theta^2(D-1)}{D(9+4k^2)} + \left[\frac{3D-2-D\tilde{R}}{3D^2}-\frac{(D-1)\tilde{R}}{D(1+2n_1)}\right]k^2\Theta^3. \tag{37}$$

The first-order correction in (37) is negative and, therefore, stabilizing, but it is also of order k^4 for long waves. The second-order correction, on the other hand, is order k^2 and can be either positive or negative, depending on the value of $\tilde{R}$. Thus, for small Θ, there is a narrow window of wavenumbers with $k\sim\Theta^{1/2}$ that can be unstable provided we satisfy a condition on $\tilde{R}$, which translates to

$$R<\left[\frac{(3D-2)(2n_1+1)}{3D^2+(2n_1-2)D}\right]^{n_1}\Theta^{n_1-1}. \tag{38}$$

The dependence on Θ mirrors our cruder prediction (28). Note that when $n_1=1$, the condition becomes $R<(3D-2)/D^2$, which indicates when unstable values of R exceed unity. The marginal curves of Fig. 5 are in agreement with the more accurate results of (38) at small Θ, as shown by the finer dotted lines in the picture.

IV. NONLINEAR DYNAMICS

Linear stability theory conveys some idea of whether small perturbations superposed on the interface of an equilibrium two-layer flow begin to amplify. Yet it says nothing about what happens subsequently to the growing modes. An unimpeded growth of the mode could lead to the breaking of interfacial waves or one of the layers collapsing and pinching off (cf. Ref. 22). We now analyze the lubrication model further to decide whether such destructive phenomena arise.

Downloaded 15 Feb 2006 to 137.82.49.199. Redistribution subject to AIP license or copyright, see http://pof.aip.org/pof/copyright.jsp

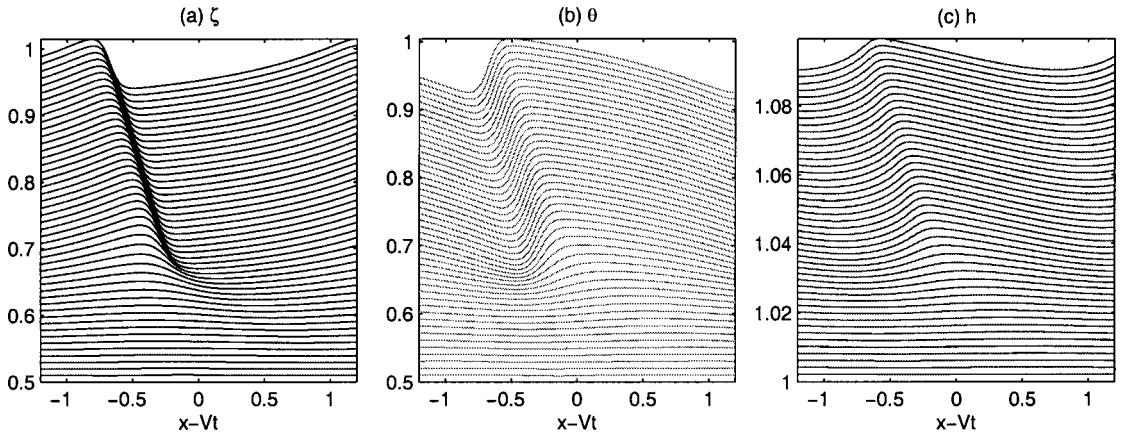

FIG. 7. A numerical solution of (24) and (25) for $\Theta=0.5$, $D=1.1$, $R=0.5$, and $n_1=n_2=1$, in a domain of size $l=2$. This flow lies just beyond the onset of interfacial instability. Shown are snapshots of (a) ζ, (b) θ, and (c) h, every 40 time units. The snapshots are shown in a frame moving with a velocity, V, close to the nonlinear wave speed to eliminate rapid propagation effects and bring out the slower growth and saturation of the mode; the snapshots are also successively offset to emphasize this pattern of evolution. Note that the offset for h is much smaller than that for ζ and θ, and the disturbance of the free surface is relatively small.

We use two computational schemes (a pseudospectral method and one based on finite differences) to numerically solve the partial differential equations of the model as initial-value problems in periodic domains in x; we state the initial conditions below. We also look for steadily propagating nonlinear waves by posing the dependences, $\zeta(x-ct)$ and $\theta(x-ct)$, and solving the resulting ordinary differential, periodic boundary-value problem, in which the wavespeed c appears as an eigenvalue.

We illustrate the dynamics for two Newtonian layers ($n_1=n_2=1$). In Fig. 7, we show a sample numerical solution in which the system is initialized with an equilibrium flow plus a low-amplitude disturbance taking the form of the unstable mode (the initial amplitude is 10^{-4}, as measured by the maximum of $|\zeta-Z|$). The picture illustrates how the unstable mode grows and then saturates at finite amplitude; the perturbation to the free surface remains small throughout, reflecting the interfacial character of the instability. The final saturated state agrees with a direct computation of the steadily propagating nonlinear wave. Moreover, when we vary parameters (such as R) to trace the nonlinear solution back to the point of neutral stability, we find its peak-to-peak amplitude decreases smoothly to zero, indicating a supercritical bifurcation (see Fig. 8). Near onset, the nonlinear wave branch can be constructed analytically using weakly nonlinear theory; this furnishes a Landau equation, $A_t=\gamma A-\Gamma|A|^2A$, determining the amplitude, $A(T)$, of the nonlinear wave, where γ is the modal growth rate and Γ is a constant given by the system parameters (e.g., Ref. 23). The weakly nonlinear result, $|A|=[\Re(\gamma/\Gamma)]^{1/2}$, is also shown in Fig. 8.

To determine whether instabilities always saturate quickly beyond onset [i.e., supercritically, with $\Re(\Gamma)>0$], we have surveyed the sign of the cubic coefficient, Γ, of the Landau equation over the four-dimensional parameter space ($D>1$, R, $0<\Theta<1$ and the domain size l). We have found no instances in which the coefficient indicates a sharper [i.e., sub-critical, with $\Re(\Gamma)<0$] transition, although a simple analytical proof of supercriticality has eluded us. Thus, low-amplitude nonlinear waves form beyond onset, and the layer structure remains intact.

Further from onset, one side of the nonlinear waves steepens to become a sharp, shock-like feature, while the other side flattens and develops a broad plateau (see Fig. 9). This latter feature becomes extensive in large domains and begins to resemble an uniform equilibrium profile with a different Θ. Because such states are unstable, we anticipate that the nonlinear waves of Fig. 9 eventually become unstable to waves growing on the plateau once l is sufficiently large. The prediction is verified by numerically solving initial-value problems that begin from states close to the steady nonlinear wave, and by computations of the linear stability of steadily propagating solutions like those in Fig. 9.

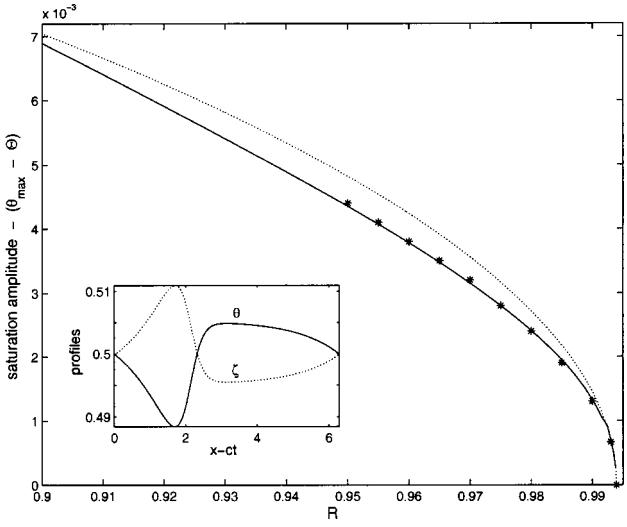

FIG. 8. Saturation amplitudes, expressed as the maximum of $\theta-\Theta$, against R for solutions of the periodic boundary-value problem for steadily propagating waves (solid), and from the end-state of initial-value computations that begin from low-amplitude random perturbations superposed on the equilibrium flow (stars). The dotted line shows the saturation amplitude expected from weakly nonlinear theory. $\Theta=1/2$, $l=2\pi$, and $D=1.1$. The inset shows the steady profiles of θ and ζ at $R=0.95$.

Downloaded 15 Feb 2006 to 137.82.49.199. Redistribution subject to AIP license or copyright, see http://pof.aip.org/pof/copyright.jsp

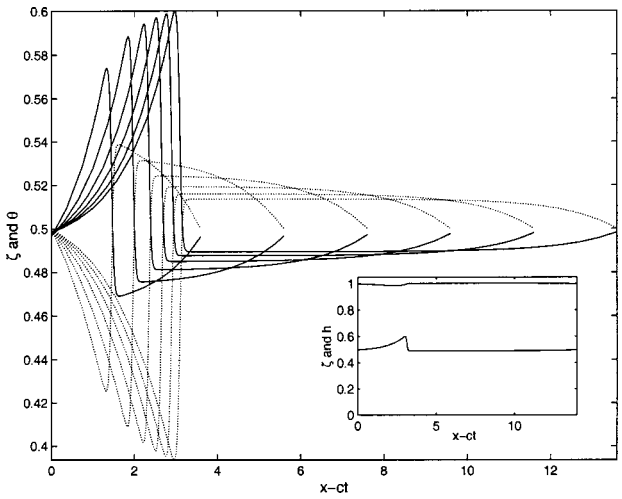

FIG. 9. Nonlinear waves in different domain lengths, l, for $\Theta=0.5$, $R=1/2$, $D=1.1$, and $n_1=n_2=1$. The solid lines show ζ, and the dotted lines show θ. The inset compares the interfacial disturbance with the free-surface distortion for the wave in the widest domain.

A sample numerical solution showing disturbances developing on a steady nonlinear interfacial wave is displayed in Fig. 10. In this example, although the system begins from a numerical solution of the boundary-value problem, small errors in the initial profile excite unstable modes. These modes take the form of secondary waves propagating across the flat plateau of the original wave; the disturbance grows to disrupt the original structure. Eventually, another peak appears, and a steady wavetrain ultimately emerges. In no cases have we found the saturation of the secondary instability at low amplitude; it invariably grows to disrupt the original nonlinear waves and spawns new peaks. We, therefore, conjecture that this instability is subcritical, and ''pulse'' generation occurs when the peaks of the original nonlinear wave are too far apart; i.e., when the domain size, l, exceeds a critical value. The critical domain size (the onset of the secondary instability) is plotted on the (d,R)-plane in Fig. 11, where d is the peak separation (which equals the domain size for a periodic wavetrain with a single peak in each period).

At first sight, it is surprising that steadily propagating multi-peak solutions are spawned in the pulse-generation events because these solutions appear by bifurcating from the uniform equilibrium flow as l varies. Yet those bifurcations are always preceded by the onset of instability to modes with fewer peaks, and so the nonlinear solutions are born unstable. In fact, by computing the linear stability of the solutions, we find that secondary instabilities also occur on these ''higher-order'' branches. The bifurcations, however, *stabilize* the multipeaked nonlinear waves on increasing l (the curves along which this stabilizing bifurcation occurs for nonlinear waves with two to four peaks are shown in Fig. 11). As the domain becomes even longer, the higher-order nonlinear waves also eventually develop wide plateaus, and so again suffer secondary instability once l becomes too large. But, over an intermediate range of domain sizes, we conclude that the multi-peaked solutions can be stable, in

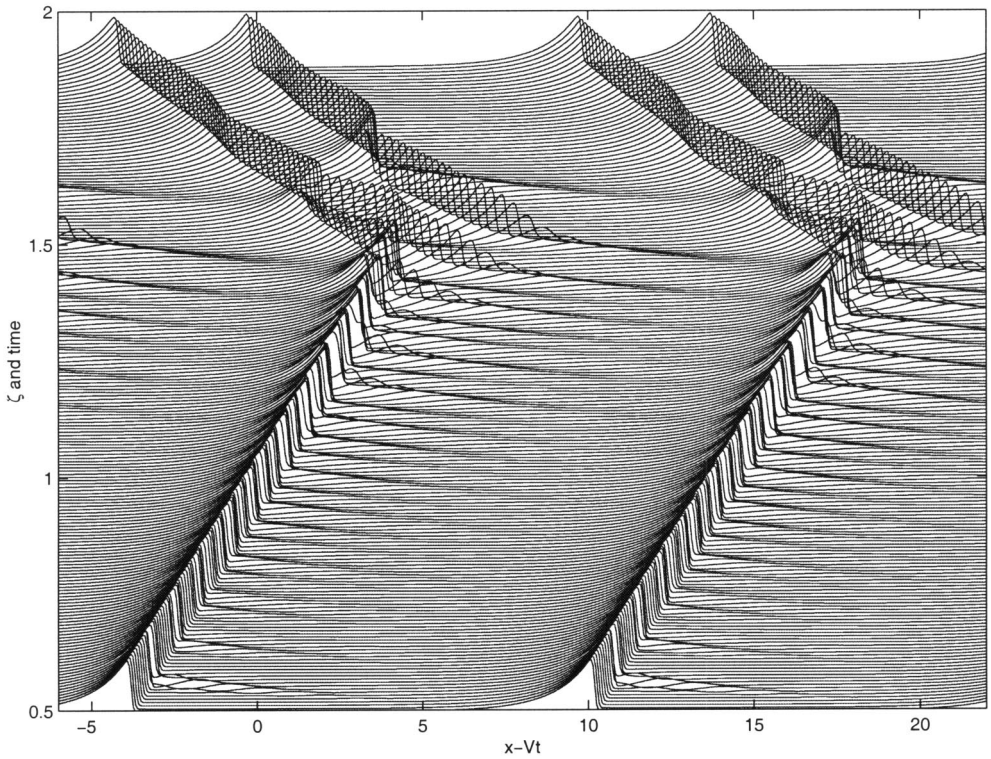

FIG. 10. A numerical solution of the initial-value problem with $\Theta=0.5$, $R=0.5$, $D=1.1$, and $n_1=n_2=1$. The initial state consists of a steady nonlinear wave in a domain of length $l=14$. The picture shows snapshots of ζ every 50 time units in a moving frame; the snapshots are successively offset to emphasize the temporal evolution. Two spatial periods are shown.

Downloaded 15 Feb 2006 to 137.82.49.199. Redistribution subject to AIP license or copyright, see http://pof.aip.org/pof/copyright.jsp

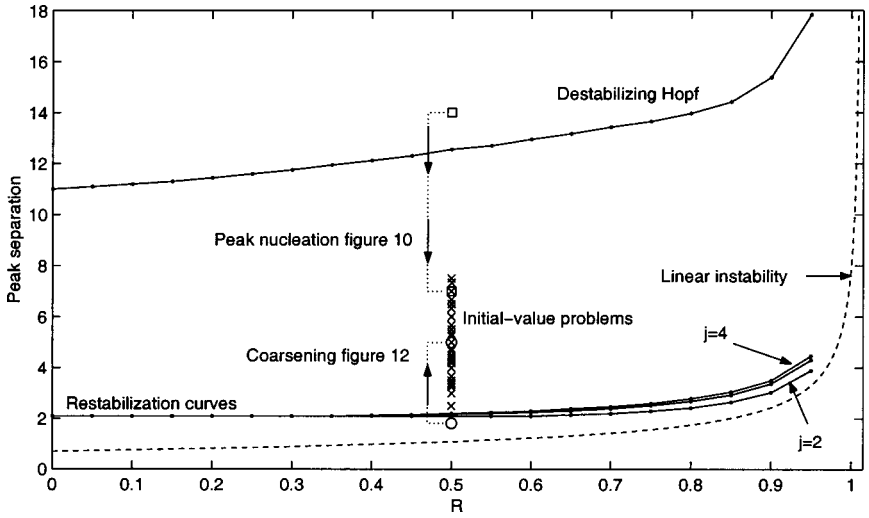

FIG. 11. A picture of the (d,R)-plane, where d is the peak separation, showing the onset of secondary instability in the primary nonlinear wave created from the uniform flow (marked "destabilizing Hopf") with $\Theta=0.5$, $D=1.1$, and $n_1=n_2=1$. Also shown is the curve along which this solution first appears (the line of linear instability of the uniform flow), and the curves where the nonlinear waves with two, three and four peaks become stabilized by a secondary bifurcation (the "restabilization curves"). The crosses mark data from the final states of the initial-value computations also shown in Fig. 13, and the circles and squares represent the peak-nucleation and coarsening simulations of Figs. 10 and 12.

accord with the final states seen after pulse-generation events.

The restabilization of the higher-order nonlinear wave branches leads to a wide range of multiple equilibria for the system in longer domains. Thus, initial-value problems beginning from low-amplitude disturbances superposed on the uniform equilibrium flow have many available end-states. In practice, we observe a selection mechanism that dictates which of the possibilities are most common: The low-amplitude noise seeds unstable modes, and that with the largest growth rate outruns the rest to create a first nonlinear structure in the domain. Typically, however, the most unstable modes have a large number of peaks, and the corresponding nonlinear solution is not stable. Consequently, the emerging nonlinear wave does not saturate, but suffers a secondary instability in which two of the peaks merge. Such pulse-merger events continue to coarsen the pattern until the number of peaks declines to the point that the relevant nonlinear wave is stable. The pattern of unstable modal growth, followed by coarsening, and then ultimate stabilization in a steady wavetrain is illustrated in Fig. 12.

The character of the selection mechanism for the peak number is illustrated further in Fig. 13, which shows results from many initial-value problems with $\Theta=R=1/2$, $D=1.1$ and $n_1=n_2=1$. In these computations, the domain length, l, varies, as does the initial condition (six low amplitude perturbations off the uniform flow with different shapes, for each value of l). The dots show the number of peaks first

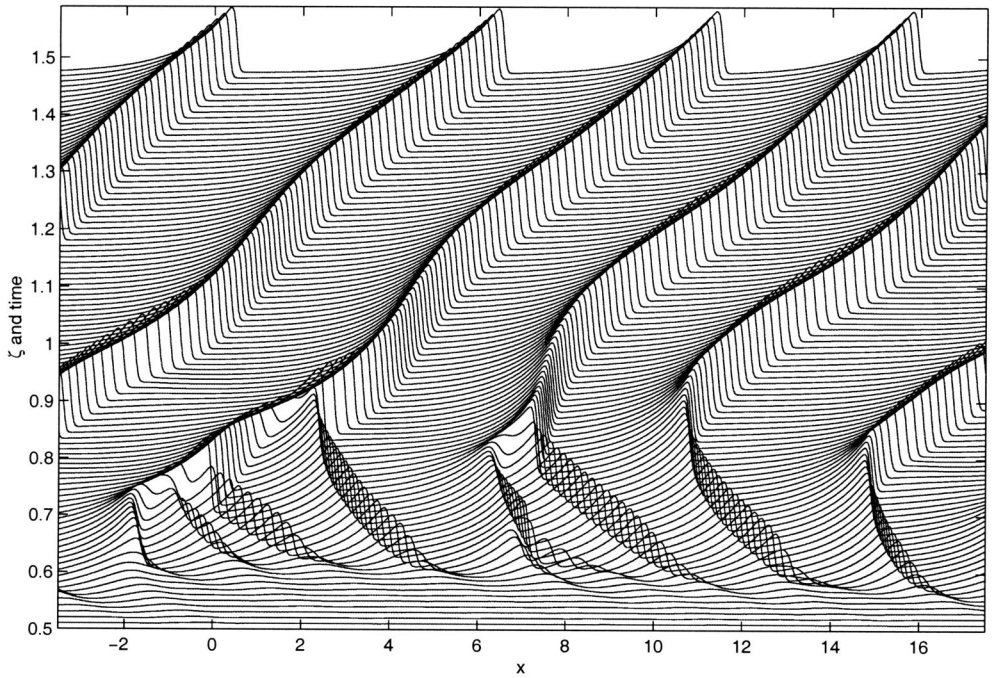

FIG. 12. A numerical solution of the initial-value problem with $\Theta=0.5$, $R=0.5$, $D=1.1$, and $n_1=n_2=1$. The initial state consists of the uniform equilibrium flow with a low-amplitude disturbance in a domain of length $l=20$. The picture shows snapshots of ζ every 40 time units in a moving frame; the snapshots are successively offset to emphasize the temporal evolution.

Downloaded 15 Feb 2006 to 137.82.49.199. Redistribution subject to AIP license or copyright, see http://pof.aip.org/pof/copyright.jsp

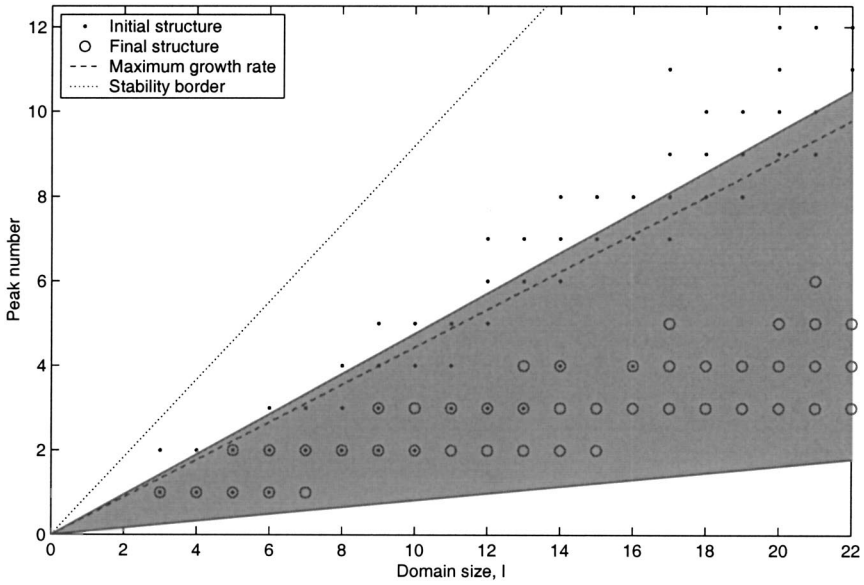

FIG. 13. A picture of the (j,l)-plane showing number of peaks, j, in solutions of initial-value problems against domain size for $\Theta=R=0.5$, $D=1.1$, and $n_1=n_2=1$. The dots show the number appearing initially, once nonlinear effects first set in; the circles show the final number (or at least that number after about 2000 time units). The initial conditions were low-amplitude perturbations about the equilibrium flow, most with rapid spatial variation, but one taking the form of the longest wave. The dotted line shows the onset of linear instability of the uniform flow, and the dashed line represents the linear mode with the largest growth rate. The shaded region, $2.1j<l<12.3j$, shows where the argument given in the main text predicts stable nonlinear waves.

appearing, and the circles show the final number (or at least that number after about 2000 time units). The figure also displays a rough criterion for stability of the final nonlinear solution, obtained as follows: The single peaked solution loses stability for $l\approx 12.3$ (see Fig. 11). We assume that this condition provides a rough criterion for when the separation between peaks becomes too large to stably support the wide intermediate plateau. Hence, the maximum domain size for a wave with j peaks is $12.3\times j$. Next, as also shown in Fig. 11, the bifurcation that restabilizes the nonlinear waves with j peaks, $j=2-4$, occurs at peak separations that are roughly independent of the peak number, j. Hence, we assume that all multi-peak solutions becomes restabilized when the peak separation is roughly 2.1 (for the current parameter settings), and so the minimum stable domain length is $2.1\times j$. The stability window predicted by this argument is shown as the shaded region in Fig. 12, and encompasses all the final states observed, with some margin above and below.

We have performed a variety of computations like those presented in this section over much wider regions of the parameter space (that is, varying Θ, D, R, n_1, and n_2). Except in cases where the lower layer was very thin (Z small) or for small R, pulse generation and coarsening dynamics are invariably found. For $Z\ll 1$ and $R\ll 1$, we observed rapid steepening into structures with very sharp shocks, as anticipated in Sec. III C. This steepening leads to resolution errors that plague detailed numerical computations in this parameter regime, and we are unable to offer a reliable description of the dynamics for these parameter settings. Nevertheless, we observed no tendency for a different kind of dynamics at small Z and R.

Kliakhandler and Sivashinsky have suggested that temporally complex interfacial dynamics can occur in multilayer flows, deriving coupled Kuramoto–Sivashinky equations in some special limits. However, in no cases have we uncovered solutions that converge to unsteady states. Overall, the behavior seems much more similar to the pulse dynamics seen in the dispersion-modified Kuramoto–Sivashinsky equation (Benney's equation) when the dispersive term is significant.[24] However, we have not systematically explored all of the parameter space to determine whether there are windows in which there is unsteady dynamics. Our conclusion is that this simply seems unlikely.

V. VERY VISCOUS UPPER LAYERS: THE ROLE OF EXTENSIONAL STRESSES

The asymptotic theory contained in preceding sections holds when the two layers have comparable effective viscosities, or at least when their ratio, R, is no larger than ϵ^{-1}, or smaller than ϵ. A large ratio is of little interest: The lower layer is so viscous that it cannot move, and the interface acts like a rigid base on the upper layer. However, the limit of small R does have physical interest, particularly in the glaciological context, where it is relevant to consider a very viscous power-law fluid, sliding over a much more fluid Newtonian layer beneath. In this situation, vertical shear in the upper layer is suppressed and the extensional stresses can become promoted into the leading-order balance of forces. These stresses are absent in the lubrication model described above, but could affect stability for $R\to 0$. Here, we will thus try to extend the theory to include extensional stresses, restricting attention to Newtonian lower layers.

A. A second lubrication model

To formulate the thin layer theory, we begin with a different asymptotic sequence for the downslope velocity in the upper layer:

$$u=u_0(x,t)+\epsilon^2 u_2(x,z,t)+\cdots, \tag{39}$$

which corresponds to near-rigid sliding. Then,

$$\dot{\gamma}_{ij}=\epsilon\begin{pmatrix} 2u_{0x} & \epsilon(u_{2z}+w_{0x}) \\ \epsilon(u_{2z}+w_{0x}) & -2u_{0x}\end{pmatrix},$$
$$\dot{\gamma}=\epsilon\sqrt{4u_{0x}^2+O(\epsilon^2)}. \tag{40}$$

Downloaded 15 Feb 2006 to 137.82.49.199. Redistribution subject to AIP license or copyright, see http://pof.aip.org/pof/copyright.jsp

To reflect the dominance of the upper-layer viscosity, while taking a distinguished limit that adds extensional stresses to the lubrication model, we set $R=\epsilon^{1+n}R_{n+1}$, giving, in the upper layer,

$$\tau_{kl}=\frac{2|u_{0x}|^{n-1}}{\epsilon R_{n+1}}\begin{pmatrix} 2u_{0x} & \epsilon(u_{2z}+w_{0x}) \\ \epsilon(u_{2z}+w_{0x}) & -2u_{0x}\end{pmatrix}, \tag{41}$$

where we lighten the notation by defining $n_1=n$. The diagonal components become order ϵ^{-1}, motivating us to define $\tilde{\tau}_{xx}=\epsilon\tau_{xx}$ and $\tilde{\tau}_{zz}=\epsilon\tau_{zz}$.

To leading order, the dimensionless governing equations may now be written in the form:

$$0=-p_x+S+\partial_z\tau_{xz}+\partial_x\tilde{\tau}_{xx}, \tag{42}$$

$$0=-p_z-1+\partial_z\tilde{\tau}_{zz}, \tag{43}$$

and the conditions at the free surface and interface as

$$h_x(\tilde{\tau}_{xx}-p)-\tau_{xz}=p-\tilde{\tau}_{zz}=0, \quad \text{on } z=h \tag{44}$$

and

$$\begin{aligned}&\tau_{xz}(x,\zeta^+,t)-2\zeta_x\tilde{\tau}_{xx}(x,\zeta^+,t)=\tau_{xz}(x,\zeta^-,t),\\ &p(x,\zeta^+,t)-\tilde{\tau}_{zz}(x,\zeta^+,t)=p(x,\zeta^-,t).\end{aligned} \tag{45}$$

We integrate to find the pressure distribution and shear stress

$$p=\tilde{\tau}_{zz}+(h-z)$$

and (46)

$$\tau_{xz}=(S-h_x)(h-z)+2\partial_x\int_z^h\tilde{\tau}_{xx}dz,$$

which imply that $p(x,\zeta^-,t)=\theta$ and

$$\tau(x,\zeta^-,t)\equiv\tau_I=(S-h_x)\theta+4R_{n+1}^{-1}\partial_x[(2|u_{0x}|)^{n-1}\theta u_{0x}], \tag{47}$$

where the last term on right-hand side is the contribution of the extensional stresses. In the equations for the evolution of the layer thicknesses (23), the ζ-equation is written much as before (but with $n_2=1$), whereas the θ-equation is evaluated immediately given that $u_0=u_I(x,t)$ is uniform in z

$$\zeta_t+\tfrac{1}{2}\partial_x[\tfrac{1}{6}\zeta^3(D-D\zeta_x-\theta_x)+u_I\zeta]=0$$

and (48)

$$\theta_t+\partial_x(u_I\theta)=0.$$

Finally, the interfacial velocity can be determined from the solution in the lower layer, given the interfacial shear stress

$$\begin{aligned}u_I=&(S-h_x)\theta\zeta+4R_{n+1}^{-1}\zeta\partial_x[(2|u_{Ix}|)^{n-1}\theta u_{Ix}]\\ &+\tfrac{1}{2}\zeta^2(D-D\zeta_x-\theta_x).\end{aligned} \tag{49}$$

This last equation is a second-order differential equation for the interfacial velocity. For reasons cited presently, we do not explore this model in detail, but construct a more general system that incorporates both versions of lubrication theory.

B. A Newtonian combined model

The explicit forms of the two versions of lubrication theory suggest a convenient combined model that captures both in different limits of R

$$\begin{aligned}&\theta_t+\partial_x[u_I\theta+\tfrac{1}{3}R(S-h_x)\theta^3]=0,\\ &\zeta_t+\tfrac{1}{2}\partial_x[u_I\zeta+\tfrac{1}{6}\zeta^3(D-D\zeta_x-\theta_x)]=0\end{aligned} \tag{50}$$

and

$$u_I=(S-h_x)\theta\zeta+4\frac{\epsilon^2}{R}\zeta\partial_x(\theta u_{Ix})+\frac{1}{2}\zeta^2(D-D\zeta_x-\theta_x). \tag{51}$$

The combined system can be crudely justified by considering a nonasymptotic extension of the lubrication model of Sec. II: One retains the higher-order extensional stresses along with the leading-order shear stresses, then evaluates them by arguing that these terms only become important for $R\gg1$, in which case the velocity field is plug-like in the upper layer and $u\approx u_I$ there. A non-Newtonian version of this theory is given presently, so we offer no further details.

With the combined model, we once more explore the linear stability of the equilibrium flow with $\zeta=Z$, $\theta=\Theta$ and $Z+\Theta=1$, using a decomposition into normal modes. Again there are two eigenvalues, one of which corresponds to an unstable mode for certain wavenumbers and parameter settings. As shown in Fig. 14, as we raise the extensional viscosity, $\eta_{ex}=\epsilon^2/R$, the associated stresses stabilize the shorter waves and reduce the range of unstable wavenumbers. However, the additional stabilization does not remove instability, but merely pushes it to longer wavelengths.

Extensional stresses also do not appear to change qualitatively the nonlinear interfacial dynamics: instabilities are invariably supercritical and saturate in steady nonlinear wavetrains beyond onset. On lengthening the domain, the wavetrains again develop wide flat plateaus, which precipitates secondary instability; coarsening and peak generation occur in larger domains to select wavetrains with peak spacings over a certain range. Figure 15 shows a selection of numerical results.

C. The non-Newtonian case

Although the Newtonian lubrication theory in (48) and (49) can be explored without difficulty [and it is not strictly necessary to proceed to the combined model in (50) and (51) in order to gauge the effect of extensional stresses], the non-Newtonian counterpart runs into some serious difficulties: The basic equilibrium state is uniform downslope, and so $u_{Ix}=0$. Thus, for $n>1$, the extensional viscosity, $4R_{n+1}^{-1}|2u_{Ix}|^{n-1}$, vanishes identically. By contrast, this viscosity is finite at $n=1$, and diverges for $n<1$. Extensional stresses therefore appear to have no effect on shear-thickening upper layers, but completely stabilize shear-thinning layers. Evidently, the system is not robust to variations in n through $n=1$.

To understand how the problem arises, we return to the governing equations, and perform a nonasymptotic expansion. We begin with the upper-layer velocity

Downloaded 15 Feb 2006 to 137.82.49.199. Redistribution subject to AIP license or copyright, see http://pof.aip.org/pof/copyright.jsp

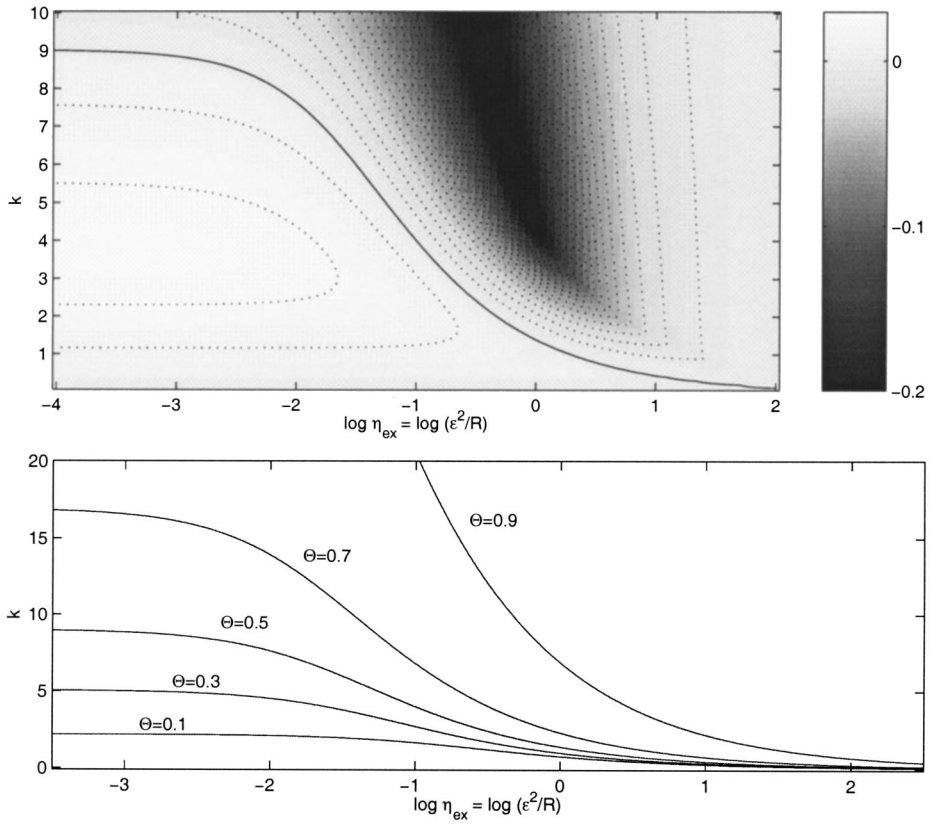

FIG. 14. Linear stability in the combined Newtonian model. The top panel shows the maximum growth rate as a density on the $(\log \eta_{ex}, k)$-plane, where $\eta_{ex}=\epsilon^2/R$, for $\Theta=1/2$, $D=1.1$ and $R=10^{-3}$. The solid line is the curve of neutral stability. The lower panel shows more curves of neutral stability on the same plane for different values of Θ (and the same R and D).

$$u=u_I(x,t)+u_\alpha(x,z,t)+\cdots, \tag{52}$$

where we fix $u_I(x,t)\sim O(1)$, but tune the order of magnitude of u_α: $u_\alpha\sim O(1)$ gives the "standard" model of Sec. IV, whereas $u_\alpha\sim O(\epsilon^2)$ leads to the model with a very viscous upper layer, as in Sec. V A.

We recall the dimensionless momentum equations to order ϵ

$$0=-p_x+S+\partial_z\tau_{xz}+\epsilon\partial_x\tau_{xx}, \tag{53}$$

$$0=-p_z-1+\epsilon\partial_z\tau_{zz}, \tag{54}$$

which retains the most important contributions of the shear stress and the extensional stresses. To the same order, the boundary and interfacial conditions are

$$h_x(\epsilon\tau_{xx}-p)-\tau_{xz}=\epsilon\tau_{zz}-p=0, \quad \text{on } z=h \tag{55}$$

and

$$\tau_{xz}(x,\zeta^+,t)-2\epsilon\zeta_x\tau_{xx}(x,\zeta^+,t)=\tau_{xz}(x,\zeta^-,t),$$
$$p(x,\zeta^+,t)-\epsilon\tau_{zz}(x,\zeta^+,t)=p(x,\zeta^-,t). \tag{56}$$

Thence,

$$p=\epsilon\tau_{zz}+h-z$$

and

$$\tau_{xz}=(S-h_x)(h-z)+2\epsilon\partial_x\int_z^h\tau_{xx}dz. \tag{57}$$

The interfacial shear stress is, therefore,

$$\tau_I=(S-h_x)\theta+2\epsilon\partial_x\int_\zeta^h\tau_{xx}dz, \tag{58}$$

which is needed to compute the lower-layer solution, with the familiar result, $u_I=\tau_I\zeta+\Delta_x\zeta^2/2$, and ζ-evolution equation in (48).

The θ-evolution equation follows from

$$0=\theta_t+\partial_x\int_\zeta^h u\,dz\equiv\theta_t+\partial_x\left(u_I\theta+\int_\zeta^h u_\alpha dz\right). \tag{59}$$

The integral of u_α in this formula is only important where $|u_{\alpha z}|\gg\epsilon^2u_{Ix}^2$. From the constitutive law and (58), truncated to order ϵ, we find an approximation

$$R^{-1}\dot\gamma^{n-1}u_{\alpha z}\approx R^{-1}u_{\alpha z}|u_{\alpha z}|^{n-1}\sim(S-h_x)(h-z). \tag{60}$$

Hence,

$$u_\alpha\approx R^{1/n}(S-h_x)^{1/n}\left[\frac{(h-z)^{1+1/n}}{1+1/n}-\frac{\theta^{1+1/n}}{1+1/n}\right], \tag{61}$$

and then

$$\theta_t+\partial_x\left[u_I\theta+\frac{nR^{1/n}}{2n+1}(S-h_x)^{1/n}\theta^{2+1/n}\right]\approx0, \tag{62}$$

which is an obvious generalization of the first relation in (50).

By contrast, the extensional stress is important where $u_{\alpha z}$ is relatively small. We introduce

$$\tau_{xx}\approx2\dot\gamma^{n-1}u_{Ix}, \quad \dot\gamma=\sqrt{\epsilon^2+4\epsilon^2u_{Ix}^2+u_{\alpha z}^2}, \tag{63}$$

Downloaded 15 Feb 2006 to 137.82.49.199. Redistribution subject to AIP license or copyright, see http://pof.aip.org/pof/copyright.jsp

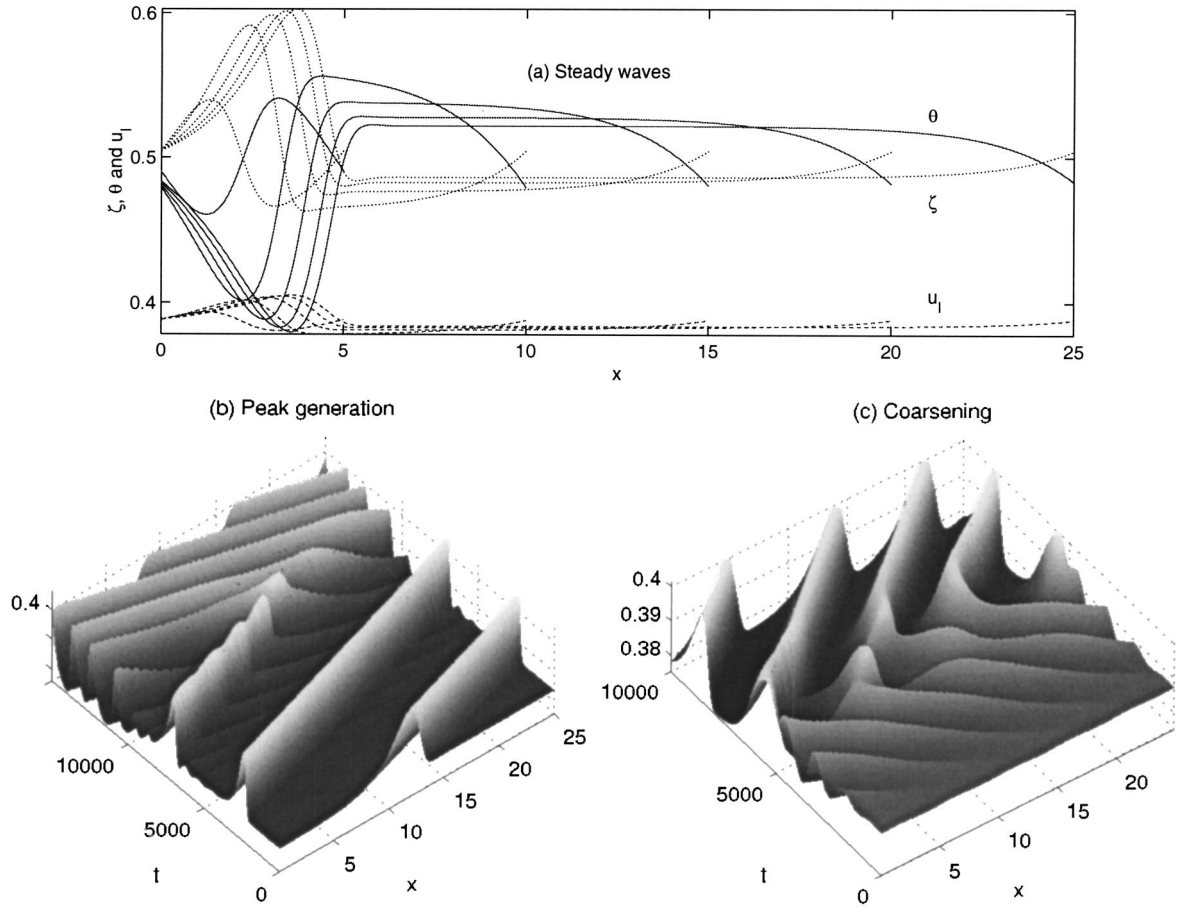

FIG. 15. Nonlinear solutions of the Newtonian combined model for $\eta_{ex}=1$, $R=0.01$, $\Theta=1/2$ and $D=1.1$. The top panel shows the steady nonlinear wave solutions that bifurcate supercritically from the uniform flow state on increasing the domain size. The lower pictures show two initial-value problems for $l=25$: In the first, the system is initialized with a steady wave with a single peak, and pulse generation occurs to yield a nonlinear wave with three peaks. In the second, the system is initialized with a low amplitude disturbance with five peaks superposed on the equilibrium flow; the disturbance grows initially to finite amplitude, but then coarsens to a steady nonlinear wave, which again has three peaks. Plotted is the interfacial speed u_I as a surface above the (x,t)-plane.

where the constant ϵ is an artificial mathematical device to regularize the viscosity should it eventually prove necessary. We then use the approximation (60) for $u_{\alpha z}$, to compute

$$\tau_I=(S-h_x)\theta+4\epsilon\partial_x(\overline{\eta}u_{Ix}), \tag{64}$$

where the depth-averaged extensional viscosity is

$$\overline{\eta}=\frac{1}{R}\int_\zeta^h \dot{\gamma}^{n-1}dz\approx\frac{1}{R}\int_\zeta^h[\epsilon^2+4\epsilon^2u_{Ix}^2+R^{2/n}(S-h_x)^{2/n}\times(h-z)^{2/n}]^{(n-1)/2}dz$$
$$=\frac{(\epsilon^2+4\epsilon^2u_{Ix}^2)^{n-1/2}}{R^2(S-h_x)}G(Y), \tag{65}$$

with

$$G(Y)=\int_0^Y(1+y^{2/n})^{(n-1)/2}dy \tag{66}$$

and

$$Y=\frac{R(S-h_x)\theta}{(\epsilon^2+4\epsilon^2u_{Ix}^2)^{n/2}}. \tag{67}$$

Hence,

$$u_I\approx(S-h_x)\theta\zeta+\frac{1}{2}\Delta_x\zeta^2+\frac{4\epsilon^2}{R^2}\zeta\partial_x\left[\frac{(\epsilon^2+4\epsilon^2u_{Ix}^2)^{n-1/2}}{(S-h_x)}G(Y)u_{Ix}\right], \tag{68}$$

which completes the system. As $\epsilon\to0$, the extensional stress disappears, leaving the original lubrication model of Sec. II. On the other hand, if $R\to0$ with ϵ^2/R fixed, the model reduces to the second lubrication theory of Sec. V A, but with a modified extensional viscosity.

The function $G(Y)$ can be written as a hypergeometric function, and has the limits

$$G(Y)\sim Y, \quad \text{for } Y\ll1 \tag{69}$$

and

Downloaded 15 Feb 2006 to 137.82.49.199. Redistribution subject to AIP license or copyright, see http://pof.aip.org/pof/copyright.jsp

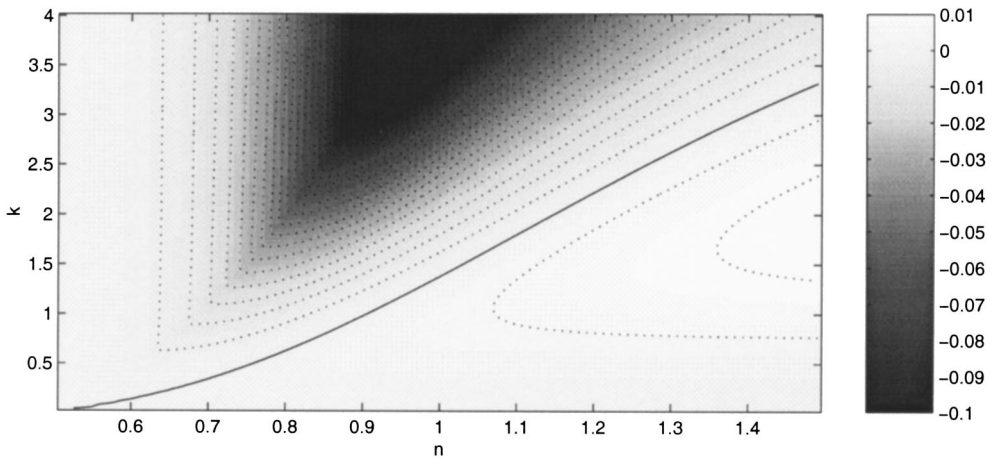

FIG. 16. Linear stability of the combined non-Newtonian model. The picture shows the maximum growth rate as a density on the (n,k)-plane, for $\Theta=1/2$, $D=1.1$, $\epsilon=0.1$, and $R=10^{-2}$. The solid line is the curve of neutral stability.

$$G(Y)\sim\begin{cases} nY^{2-1/n}/(2n-1), & n>1/2, \\ G_\infty, & n<1/2, \end{cases} \quad \text{for } Y\gg 1, \tag{70}$$

where $G_\infty(n)$ is a constant. The first limit implies that

$$u_I\to(S-h_x)\theta\zeta+\frac{1}{2}\Delta_x\zeta^2 + \frac{4\epsilon^2}{R}\zeta\partial_x[(\epsilon^2+4\epsilon^2u_{Ix}^2)^{(n-1)/2}\theta u_{Ix}], \tag{71}$$

for $R|S-h_x|\theta\ll(\epsilon^2+4\epsilon^2u_{Ix}^2)^{n/2}$, which is equivalent to (49), but for the artificial regularization, ϵ. This limit is inaccessible if $\epsilon\ll 1$ and $u_{Ix}\to 0$ (the equilibrium flow).

For the second limit, we distinguish the two cases: If $n>1/2$

$$u_I\to(S-h_x)\theta\zeta+\frac{1}{2}\Delta_x\zeta^2 + \frac{4\epsilon^2 n}{2n-1}R^{-1/n}\zeta\partial_x[(S-h_x)^{1-1/n}u_{Ix}\theta^{2-1/n}]. \tag{72}$$

But if $n<1/2$

$$u_I\to(S-h_x)\theta\zeta+\frac{1}{2}\Delta_x\zeta^2 + 4\epsilon^2R^2G_\infty\zeta\partial_x\left[(\epsilon^2+4\epsilon^2u_{Ix}^2)^{(n-1)/2}\frac{u_{Ix}}{S-h_x}\right]. \tag{73}$$

These limits are appropriate for $R|S-h_x|\theta\gg(\epsilon^2+4\epsilon^2u_{Ix}^2)^{n/2}$, and therefore, characterize small perturbations about the equilibrium flow. In fact, they also arise if one performs the lubrication-style asymptotic expansion on the linearization of the governing equations (2) and (3) (rather than linearizing the lubrication theory, as done here). Provided $n>1/2$, the extensional viscosity remains finite, and is actually given by the equilibrium vertical shear stress, which disappeared to higher order in the expansion of Sec. V A (and is contained in the term $u_{\alpha z}$ in $\dot\gamma$). Thus, the regularity of the problem is restored and we may set $\epsilon=0$. However, if $n<1/2$, as $u_{Ix}\to 0$, the extensional stress within (73) is given solely by the artificial regularizor, ϵ, signifying that there are still problems in the expansion.

In summary, if $n>1/2$, our model successfully regularizes the extensional viscosity in the limit of uniform flow; the structural instability of the model of Sec. V A arises through neglecting the equilibrium vertical shear stress. We illustrate the result with solutions of the linear stability problem: In Fig. 16, we show growth rates on the (n,k)-plane. There are no sudden changes on varying the power-law exponent through unity, and shear thinning is seen to play a stabilizing role on the unstable eigenmode (the range of unstable wavenumbers narrows as n declines). A sharp change does occur along a curved path on the (n,k)-plane, where the two eigenvalues exchange roles in regard to the size of their real parts. Note that the growth rates approach small negative values for small n, which corresponds to large extensional viscosity. The associated, nearly neutral modes describe deformations of the upper layer which are locked into place by the strong extensional stress; these modes are advected downslope with the speed, U, of the equilibrium interface, and consequently, $\lambda\to -ikU$ (a similar effect is apparent in Fig. 14).[28]

VI. CONCLUSIONS

In this article, we have explored interfacial instability in two superposed layers of power-law fluid flowing down an inclined plane. We specialized to the limit of zero Reynolds number and exploited lubrication theory to build two reduced models of the dynamics. One model is appropriate for layers with comparable effective viscosities, and we have presented a detailed discussion of the linear stability and nonlinear dynamics within the framework of this model. The second model is relevant to layers in which the upper fluid is much more viscous than the lower one. For the second model, we have verified that instability persists when the

Downloaded 15 Feb 2006 to 137.82.49.199. Redistribution subject to AIP license or copyright, see http://pof.aip.org/pof/copyright.jsp

fluids are Newtonian; extensional stresses act to stabilize shorter wavelength perturbations of the interface, but cannot remove instability entirely.

One surprise of the second theory is that it proves difficult to offer a self-consistent stability theory for a non-Newtonian upper layer. This arises because the equilibrium state about which we perform the stability analysis has zero strain rate to leading order. A shear-thinning fluid then possesses an infinite extensional viscosity, and a shear-thickening fluid has zero extensional viscosity. Hence, the slightest variations in the rheological law near the Newtonian limit completely changes the extensional viscosity and the model is not robust. Part of the problem lies in the fact that the vertical shear rate in the second model appears only at higher order, and in practice this can regularize the viscosity. We have presented a version of the asymptotic theory that brings out this special feature of the problem and allows a physically plausible stability analysis for a range of non-Newtonian materials. However, even this theory breaks down for very shear-thinning materials, and we have no option other than regularizing the viscosity of the non-Newtonian fluid model so that it never truly diverges (a popular approach in non-Newtonian fluid mechanics where it is often argued that the power-law rheological model is not physically correct at zero strain-rate). From the mathematical perspective, it remains to be seen whether we have exposed a flaw in thin-layer theory, or found a basic problem in the linear stability analysis.

Finally, we return to the ice-flow problem, and discuss the relevance of our results to ice streams. There are two major problems in attempting to rationalize such structures in terms of finger-like interfacial instabilities. First, although we are able to generalize the lubrication model to three-dimensional superposed layers, the linear stability theory predicts that instabilities with the correct spatial structure are atypical (that is, unstable modes with dependence $\exp[ikx+ily+\lambda t]$ and $k \gg l$); patterns with comparable variations in x and y (the direction across the plane) are usually preferred.[25] Thus interfacial instabilities seem more relevant to ''wavy'' ice formations rather than streams, which probably have a partly thermal origin.[26] Second, ice rheology is commonly modelled as a power-law fluid with $n<1/2$. Thus all the problems in the thin-layer model likely apply to the glacial application unless the lower layer over which the ice slides has comparable viscosity, which seems unlikely. Even so, our results suggest that strong extensional viscosities may well stabilize interfacial instability in these configurations.

ACKNOWLEDGMENTS

This work began at the 2001 GFD Summer Study Program, Woods Hole Oceanographic Institution (which is supported by NSF and ONR). We thank the participants, and expecially Eli Tziperman, for discussions. N.J.B. and C.T. were supported by the National Science Foundation (Grant No. DMS 72521).

[1] C. S. Yih, ''Instability due to viscosity stratification,'' J. Fluid Mech. **27**, 337 (1967).
[2] T. B. Benjamin, ''Wave formation in laminar flow down an inclined plane,'' J. Fluid Mech. **2**, 554 (1957); corrigendum **3**, 657 (1957).
[3] D. J. Benney, ''Long waves on liquid films,'' J. Math. Phys. (Cambridge, Mass.) **45**, 150 (1966).
[4] H.-C. Chang, ''Wave evolution on a falling film,'' Annu. Rev. Fluid Mech. **26**, 103 (1994).
[5] K. P. Chen, ''Wave formation in the gravity-driven low-Reynolds number flow of two liquid films down an inclined plane,'' Phys. Fluids A **5**, 3038 (1993).
[6] S. J. Weinstein, ''Wave propagation in the flow of shear-thinning fluids down an incline,'' AIChE J. **36**, 1873 (1990).
[7] A. P. Hooper and W. G. C. Boyd, ''Shear-flow instability at the interface between two viscous fluids,'' J. Fluid Mech. **128**, 507 (1983).
[8] F. Charru and E. J. Hinch, ''Phase diagram of interfacial instabilities in a two-layer Couette flow and mechanism of the long-wave instability,'' J. Fluid Mech. **414**, 195 (2000).
[9] D. S. Loewenhertz and C. J. Lawrence, ''The effect of viscosity stratification on the stability of a free surface flow at low Reynolds numbers,'' Phys. Fluids A **1**, 1686 (1989).
[10] I. L. Kliakhandler and G. I. Sivashinsky, ''Viscous damping and instabilities in stratified liquid flowing down a slightly inclined plane,'' Phys. Fluids **9**, 23 (1997).
[11] N. D. Waters, ''The stability of two stratified power-law liquids in Couette flow,'' J. Non-Newtonian Fluid Mech. **12**, 85 (1983).
[12] B. Khomami, ''Interfacial stability and deformation of two stratified power law fluids in plane Poiseuille flow. 1. Stability analysis,'' J. Non-Newtonian Fluid Mech. **36**, 289 (1990).
[13] H. Engelhardt, N. Humphrey, B. Kamb, and M. Fahnestock, ''Physical conditions at the base of a fast moving Antarctic ice stream,'' Science **248**, 57 (1990).
[14] D. S. Loewenhertz, C. J. Lawrence, and R. L. Weaver, ''On the development of transverse ridges on rock glaciers,'' J. Glaciol. **35**, 383 (1989).
[15] W. S. B. Paterson, *The Physics of Glaciers* (Butterworth-Heinemann, Oxford, 1998).
[16] B. T. Erneux and S. H. Davis, ''Nonlinear rupture of free films,'' Phys. Fluids A **5**, 1117 (1993).
[17] D. T. Papageorgiou, ''Analytical description of the breakup of liquid jets,'' J. Fluid Mech. **301**, 109 (1995).
[18] D. R. MacAyeal, ''Large-scale ice flow over a viscous basal sediment: Theory and application to ice stream B, Antarctica,'' J. Geophys. Res., [Solid Earth Planets] **94**, 4071 (1989).
[19] T. W. Kao, ''Role of the interface in the stability of stratified flow down an inclined plane,'' Phys. Fluids **8**, 2190 (1965).
[20] T. W. Kao, ''Stability of two-layer viscous stratified flow down an inclined plane,'' Phys. Fluids **8**, 812 (1965).
[21] T. W. Kao, ''Role of viscosity stratification in the stability of two-layer flow down an incline,'' J. Fluid Mech. **33**, 561 (1968).
[22] C. Pozrikidis, ''Gravity-driven creeping flow of two adjacent layers through a channel and down a plane wall,'' J. Fluid Mech. **371**, 345 (1998).
[23] P. Manneville, *Dissipative Structures and Weak Turbulence* (Academic, San Diego, CA, 1990).
[24] N. J. Balmforth, G. R. Ierley, and R. Worthing, ''Pulse dynamics in an unstable medium,'' SIAM (Soc. Ind. Appl. Math.) J. Appl. Math. **57**, 205 (1997).
[25] C. Toniolo, ''Slipping instability in two-layer flows,''in *Proceedings of the 2001 GFD Summer School*, Woods Hole Oceanographic Institution (WHOI, Woods Hole, MA, 2001).
[26] A. C. Fowler, ''Ice-sheet surging and ice-stream formation,'' Ann. Glaciol. **23**, 68 (1996).
[27] The criteria in (28) and (30) turn out to be exact if $D=1$.
[28] We emphasize that the linear stability results of this section are consistent solutions of the lubrication limit of the problem: As mentioned earlier, the linear theory obtained from the regularized model is identical to that which results if one first linearizes the governing equations about the basic equilibrium flow, and then applies the lubrication approximation (which automatically ensures that the extensional viscosity is given by the vertical shear of the equilibrium flow). Hence, the results do not rely on the cruder regularization adopted in this subsection, which we offer as a nonlinear generalization.

Downloaded 15 Feb 2006 to 137.82.49.199. Redistribution subject to AIP license or copyright, see http://pof.aip.org/pof/copyright.jsp